

Optimize Purcell filter design for reducing influence of fabrication variation

Xiao Cai(蔡晓), Yi-Biao Zhou(周翼彪), Wen-Long Yu(于文龙), Kang-Lin Xiong(熊康林), and Jia-Gui Feng(冯加贵)

Citation: Chin. Phys. B, 2024, 33 (**6**): 068501. DOI: 10.1088/1674-1056/ad3345
Journal homepage: http://cpb.iphy.ac.cn; http://iopscience.iop.org/cpb

What follows is a list of articles you may be interested in

Characterization of topological phase of superlattices in superconducting circuits

Jianfei Chen(陈健菲), Chaohua Wu(吴超华), Jingtao Fan(樊景涛), and Gang Chen(陈刚)
Chin. Phys. B, 2022, 31 (**8**): 088501. DOI: 10.1088/1674-1056/ac5612

Shortcut-based quantum gates on superconducting qubits in circuit QED

Zheng-Yin Zhao(赵正印), Run-Ying Yan(闫润瑛), and Zhi-Bo Feng(冯志波)
Chin. Phys. B, 2021, 30 (**8**): 088501. DOI: 10.1088/1674-1056/abea96

Fabrication and characterization of all-Nb lumped-element Josephson parametric amplifiers

Hang Xue(薛航), Zhirong Lin(林志荣), Wenbing Jiang(江文兵), Zhengqi Niu(牛铮琦), Kuang Liu(刘匡), Wei Peng(彭炜), and Zhen Wang(王镇)
Chin. Phys. B, 2021, 30 (**6**): 068503. DOI: 10.1088/1674-1056/abeee6

Controllable microwave frequency comb generation in a tunable superconducting coplanar-waveguide resonator

Shuai-Peng Wang(王帅鹏), Zhen Chen(陈臻), and Tiefu Li(李铁夫)
Chin. Phys. B, 2021, 30 (**4**): 048501. DOI: 10.1088/1674-1056/abc2bb

Superconducting tunable filter with constant bandwidth using coplanar waveguide resonators

Ying Jiang(蒋莹), Bo Li(李博), Bin Wei(魏斌), Xu-Bo Guo(郭旭波), Bi-Song Cao(曹必松), Li-Nan Jiang(姜立楠)
Chin. Phys. B, 2017, 26 (**10**): 108501. DOI: 10.1088/1674-1056/26/10/108501

Optimize Purcell filter design for reducing influence of fabrication variation

Xiao Cai(蔡晓)[1], Yi-Biao Zhou(周翼彪)[2], Wen-Long Yu(于文龙)[1], Kang-Lin Xiong(熊康林)[1,2], and Jia-Gui Feng(冯加贵)[1,2,†]

[1] *Gusu Laboratory of Materials, Suzhou* 215123, *China*
[2] *Suzhou Institute of Nano-Tech and Nano-Bionics, Chinese Academy of Sciences, Suzhou* 215123, *China*

(Received 25 December 2023; revised manuscript received 25 February 2024; accepted manuscript online 13 March 2024)

To protect superconducting qubits and enable rapid readout, optimally designed Purcell filters are essential. To suppress the off-resonant driving of untargeted readout resonators, individual Purcell filters are used for each readout resonator. However, achieving consistent frequency between a readout resonator and a Purcell filter is a significant challenge. A systematic computational analysis is conducted to investigate how fabrication variation affects filter performance, through focusing on the coupling capacitor structure and coplanar waveguide (CPW) transmission line specifications. The results indicate that the T-type enclosing capacitor (EC), which exhibits lower structural sensitivity, is more advantageous for achieving target capacitance than the C-type EC and the interdigital capacitor (IDC). By utilizing a large-sized CPW with the T-type EC structure, fluctuations in the effective coupling strength can be reduced to 10%, given typical micro-nanofabrication variances. The numerical simulations presented in this work minimize the influence of fabrication deviations, thereby significantly improving the reliability of Purcell filter designs.

Keywords: superconducting circuit, Purcell filter, coplanar waveguide, capacitor structure

PACS: 85.25.Am, 84.30.Vn, 84.32.Tt, 03.67.Lx **DOI:** 10.1088/1674-1056/ad3345

1. Introduction

Quantum computing systems based on superconducting circuits have received substantial attention due to their flexibility in design and the potential for integration through micro-nanofabrication technology.[1] However, quantum states are delicate and susceptible to environmental noise and various types of losses. Therefore, it is imperative to understand the decoherence mechanisms and optimize the circuit design to achieve high-fidelity qubit state readout and control. There are many mechanisms affecting qubit lifetime,[2,3] including losses induced by two-level system (TLS),[2,4,5] Purcell effect,[6,7] and quasiparticles (QP).[8,9] The energy relaxation rate Γ_1 is given by

$$\Gamma_1 = \frac{1}{T_1} = \Gamma_{\rm TLS} + \Gamma_{\rm QP} + \Gamma_{\rm Purcell} + \Gamma_{\rm Other}. \tag{1}$$

Purcell effect is a crucial mechanism of loss, and it refers to the coupling of a qubit with external circuits through a resonator. This coupling leads to the emission of photons from the qubit into the environment, thereby reducing the coherence time of superconducting qubits.

In recent years, researchers have explored various band-pass or band-stop filters to inhibit the Purcell effect.[10–17] Purcell filters include the widely used $\lambda/4$ resonant filters,[13] the $\lambda/2$ CPW resonator,[18] and filters explored by Bronn *et al.*,[19] Reed *et al.*[7] and Heinsoo *et al.*[20] These filters differ in their coupling characteristics, bandwidth, footprint structure, and performance stability. Heinsoo *et al.*[20] implemented a $\lambda/4$ filter with the same resonant frequency as the readout resonator to achieve improved suppression while maintaining good readout efficiency. The implementation challenge of the filter lies in achieving consistent resonant frequency in a stable and reliable manner between the readout resonator and the Purcell filter. As is well known, excessive or insufficient etching of the edges of the pattern may lead to pattern deviation in the fabricating process. Therefore, the variations in capacitance and inductance break frequency consistency of expected design and lead to poor filter performance. These fabrication deviations exhibit spatial randomness in the preparation process and have statistical patterns. However, it is a challenge to accurately quantify and eliminate them in a single preparation. Recently, researchers used a set of air bridges to adjust the frequency of the CPW resonator, achieving frequency matching between the readout resonator and the Purcell filter.[21] To avoid trials and errors in experiments, this work combines the circuit simulations and the finite element calculations to analyze the microwave transmission characteristics and coupling structure design of the Purcell filter (Heinsoo *et al.*[20]) under graphical edge etching deviations. This study provides design guidance for optimizing the structure of the CPW, filters, and feed lines, so as to significantly improve the performance stability of the Purcell filter.

†Corresponding author. E-mail: jgfeng2017@sinano.ac.cn

© 2024 Chinese Physical Society and IOP Publishing Ltd

2. Filter structure and transmission characteristics

Based on the microwave circuit theory, the relaxation rate of qubits induced by external circuits is related to the qubit capacitance and the input impedance of the external circuit, which can be related by[7]

$$T_{1,\mathrm{Purcell}} = \frac{C_\mathrm{q}}{\mathrm{Re}\left(Y\left(\omega_\mathrm{q}\right)\right)}, \tag{2}$$

where C_q represents the qubit capacitance, and Y denotes the admittance from the qubit observation to the external circuit. The transmission line circuit models of four different Purcell filters (Figs. 1(a)–1(d)) are established. As depicted in Fig. 1, the readout resonator frequency ω_p is 6.3 GHz, and the qubit capacitance C_q is 80 fF. The coupling capacitance C_g between qubit and resonator is 5 fF. The coupling capacitance C_k between feedline and resonator is 12 fF, and its quality factor $Q_\mathrm{c} \sim 3000$. Using Eq. (2), the values of $T_{1,\mathrm{Purcell}}$ at different qubit frequencies are obtained. Without the protection of Purcell filter, the qubit lifetime is limited by Purcell effect. Filter C can provide excellent protection of qubits in a narrow frequency band. Filter B shows improved performance in a wider range of frequencies. Filter D demonstrates the best results and $T_{1,\mathrm{Purcell}}$ exceeds 1 s when the qubit frequency is below 5 GHz. In the commonly used filters A and B, the filter bandwidth is much greater than the readout resonator bandwidth, resulting in relaxed requirements for fabrication tolerances. However, in filter D, both bandwidths are small and comparable to each other, making the design extremely sensitive to fabrication errors. Next, the structural characteristics about filter D is analyzed.

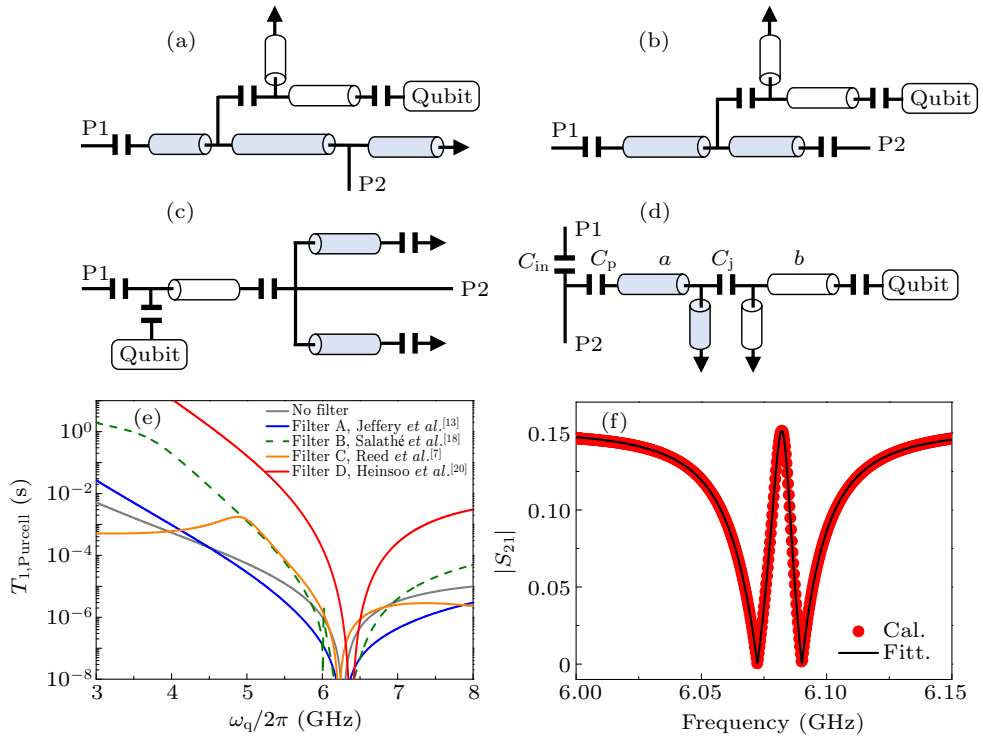


Fig. 1. (a)–(d) Schematic diagrams of filters A, B, C, and D, with light blue parts being main structures of filters; (e) variations of lifetime $T_{1,\mathrm{Purcell}}$ of qubit with frequency under protection of Purcell filters, (f) typical S_{21} curve with two dips for filter D. The red dot data comes from the circuit simulation model, and the black curve is fitted according to Eq. (3).

As shown in Figs. 1(d) and 1(f), the filter system comprises two distributed $\lambda/4$ resonant cavities with identical frequencies, a capacitor of C_in, a coupling capacitor C_p between the transmission line and the filter, and a coupling capacitor of C_j between the filter and the readout resonator. The capacitor C_in ensures that the majority of reflected signals from the resonant resonator can reach port P2.[20] The capacitor C_p determines the coupling strength between the filter and the transmission line, and the capacitor C_j determines the coupling strength between the filter and the readout resonator. When the capacitors are well designed, the S_{21} curve obtained by circuit model displays two dips.

Heisnoo *et al.*[20] analyzed each coupling parameter in the circuit (including the resonant frequencies of the filter and the readout resonator) by using the input–output theory. This analysis is performed by fitting the following equation

$$\frac{S_{21}}{1-\Gamma} = 1 - \frac{1+\Gamma}{1+\mathrm{Re}(\Gamma)} \times \frac{\tilde{\kappa}_a(\gamma_b + 2\mathrm{i}\Delta_b + \kappa_b)}{4J^2 + (\gamma_a + 2\mathrm{i}\tilde{\Delta}_a + \tilde{\kappa}_a)(\gamma_b + 2\mathrm{i}\Delta_b + \kappa_b)}, \tag{3}$$

where Γ is the reflection coefficient of the port P1, $\tilde{\kappa}_a$ is the linewidth after taking into account the environment, γ_a and γ_b are the intrinsic dissipation rates of the resonant cavities a and b, Δ_a (Δ_b) is the detuning between the driving frequency of

the input field and the bare resonant frequency a (b) of the respective mode, κ_a is the coupling strength between the Purcell filter and the feedline, κ_b is the weaker coupling strength between the readout resonator and the qubit driving line, J is the coupling strength between the Purcell filter and the readout resonator. The focus is on the following system parameters: filter frequency ω_p, readout resonator frequency ω_r, filter bandwidth κ_p, filter-readout resonator coupling strength J, and the effective coupling strength κ_eff for evaluating the readout efficiency of the readout resonator.

$$\kappa_\mathrm{eff} = \frac{1}{2}\left(\kappa_\mathrm{p} - \mathrm{Re}\left\{\sqrt{-16J^2 + \left(\kappa_\mathrm{p} - 2\mathrm{i}(\omega_\mathrm{R} - \omega_\mathrm{p})\right)^2}\right\}\right). \quad (4)$$

Figure 1(f) shows a typical S_{21} curve for filter D system with $J/2\pi = 8.8$ MHz, $\omega_\mathrm{r}/2\pi = \omega_\mathrm{p}/2\pi = 6.08$ GHz, and $\kappa_\mathrm{p}/2\pi = 45.5$ MHz. The split occurs when the two resonator frequencies are aligned and the size of the split depends on the coupling strength J, while the symmetry of the split valley is related to the alignment of the two frequencies. According to Eq. (4), J and the frequency consistency determine the effective coupling strength κ_eff. The κ_eff tends to be maximized when $\omega_\mathrm{r} = \omega_\mathrm{p}$, which is very important for fast readout.

3. Sensitivity analysis of coupling capacitance

The first step is to establish a microwave transmission line model of the filter system. The rapid scanning analysis is performed on various system parameters. Figure 2 illustrates the influence of fabrication tolerance on the coupling capacitances C_p and C_j in comparison with an initial design ($C_\mathrm{p} = 36$ fF, $C_\mathrm{j} = 2$ fF). As depicted in Fig. 2(a), it is clear that the deviation of C_p from its design value (36 ± 4 fF $\sim \pm 11\%$) can significantly influence the filter frequency and lead to a breaking of the symmetry of the S_{21} curve, which should be strictly avoided in the device design stage. On the other hand, the deviation of C_j from its design value (2 ± 1 fF $\sim \pm 50\%$) has a limited effect on the symmetry of the double dips (as shown in Fig. 2(b)), but it does alter the separation between the two dips.

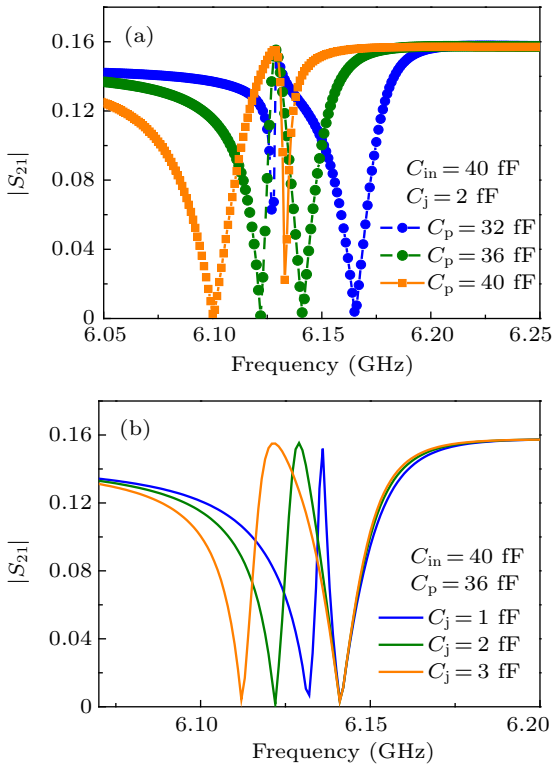


Fig. 2. Analysis of Purcell filter parameters: (a) C_p ranging from 32 fF to 40 fF and (b) C_j ranging from 1 fF to 3 fF, with single factor scanning used. The initial values are $\omega_\mathrm{r} = \omega_\mathrm{p} \sim 6$ GHz, $C_\mathrm{in} = 40$ fF, $C_\mathrm{p} = 36$ fF, and $C_\mathrm{j} = 2$ fF.

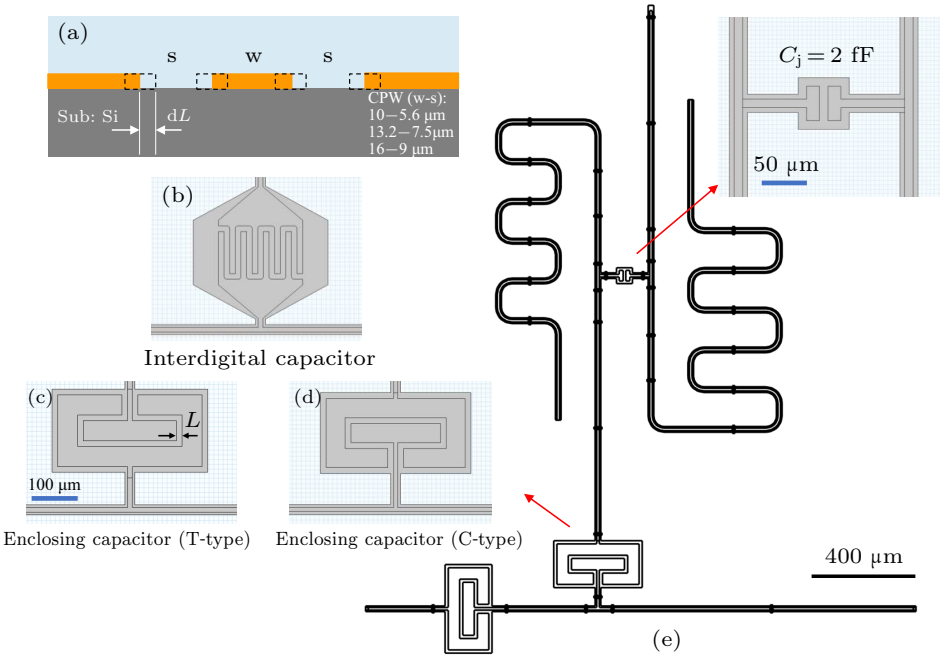


Fig. 3. Typical design of Purcell filter in finite element calculations with parameters $C_\mathrm{in} = C_\mathrm{p} = 40$ fF, $C_\mathrm{j} = 2$ fF, showing (a) CPW etching error diagram, (b) interdigital capacitor, (c) C-type capacitor, (d) T-type capacitor, (e) sensitivity analysis of coupling parameters by adjusting structures of the CPW and coupling region (C_p).

Typically, the primary source of capacitance deviations in the system stems from excessive or insufficient etching of the pattern edges in the fabrication process. To simplify computational analysis, we assume that all pattern edges exhibit uniform etching error behaviors within a single fabrication process. Finite element calculations are employed to design an interdigital capacitor with a capacitance of 40 fF. This structure features a finger and gap width of 6 μm, a finger length of 100 μm, and a footprint size of 124 μm×270 μm. The calculation results reveal that the capacitance sensitivity to pattern edge etching deviations is about 4.5 fF/μm.[22] In the related experiments, the actual finger width is measured to be in a range between 4.8 μm and 5.4 μm. The combination of these calculation results and experimental measurements indicate that the fabrication process can result in a maximum deviation of 5.4 fF in the actual capacitance, potentially significantly affecting device performance. In the present process, ensuring the stability and reliability of capacitors $C_{\rm p}$ and $C_{\rm in}$ is a major challenge. One strategy to reduce sensitivity is to increase the characteristic size (L) of the capacitor. With an L of 12 μm, the capacitance sensitivity of the interdigital capacitor decreases to about 2.1 fF/μm, and the overall device size is 250 μm×317 μm, 2.3 times larger than the previous pattern. Another strategy involves the use of an enclosing capacitor[23–25] as depicted in Fig. 3. The enclosing capacitor, with its large block area, is less sensitive to edge fluctuations. Moreover, the size of enclosing capacitor is much smaller. Finite element calculations show that the capacitance sensitivity is 3.5 fF/μm (1.8 fF/μm) for $L = 6$ μm ($L = 12$ μm).

4. Synthetic design of Purcell filter

In the filter system, an enclosing capacitor is utilized for the coupling structure $C_{\rm p}$ as depicted in Fig. 3, due to the sensitivity characteristics of capacitors. The C-type and T-type capacitors are designed based on the different opening directions surrounding electrode structure. Specifically, the opening of the C-type capacitor is directed towards the transmission line, and the opening of T-type capacitor towards the filter. To achieve a relatively small capacitance $C_{\rm j}$ between the resonant resonator and the filter, two rectangular designs are employed. Our computational model takes into account the enclosing capacitors and the interdigital capacitor, each with a characteristic size (L) of 12 μm. Additionally, we consider three types of CPW structures. These CPWs are characterized by trace width (w) and clearance (s), with a characteristic impedance of 50 Ω and dimensions of 10 μm–5.6 μm, 13.2 μm–7.5 μm, and 16 μm–9 μm, respectively. The pattern edge deviation in the fabrication process is denoted as dL, and the filter structure is systematically analyzed at an interval of ±0.5 μm for dL. A silicon (Si) substrate, with a dielectric constant of 11.5, is employed in this study.

Prior to conducting the extensive numerical calculations, we determine the appropriate grid size for the relevant core pattern region to ensure the model's grid independence. Utilizing finite element calculations, the system parameters are extracted by fitting the S_{21} curve through using Eq. (3) as depicted in Figs. 4(a), 4(c), and 4(e). Under the ideal design condition (d$L = 0$ μm), we achieve the optimal coupling parameters. The fitting result yields $\kappa_{\rm eff}/2\pi \sim 20$ MHz and $\omega_{\rm r} - \omega_{\rm p} \sim 0$ MHz. From our previous analysis, it is clear that $C_{\rm p}$ experiences fluctuations in the presence of excessive etching or insufficient etching deviations. Consequently, $\kappa_{\rm eff}$ decreases sharply as fabrication variation increases. The comparison between the C-type capacitor and the interdigital capacitor shows that the $\kappa_{\rm eff}$ fluctuation with a T-type capacitor can be reduced by 20%–40% under the same CPW condition. On the other hand, the calculation results indicate that increasing the size of the CPW helps mitigate the influence of etching deviations on the coupling strength. For example, in the d$L = \pm 0.5$ μm range, a T-type capacitor with 10 μm–5.6 μm CPW shows a significant $\kappa_{\rm eff}$ fluctuation: 0%–60%. However, a T-type capacitor with 16 μm–9 μm CPW shows only 0%–10% $\kappa_{\rm eff}$ fluctuation in the same dL range, and the frequency difference $\omega_{\rm r} - \omega_{\rm p}$ achieves the mildest fluctuation (< 10 MHz).

Figures 4(b), 4(d), and 4(f) show the average values and standard deviations of the coupling parameters at a dL interval of ±0.5 μm. This provides an alternative perspective to examine the relationship between key structural combinations of filter and the stability of microwave characteristic. In the three capacitor designs, it is evident that the fluctuations of the system parameters $\kappa_{\rm eff}$ and $\omega_{\rm r} - \omega_{\rm p}$ linearly decrease as the size of the CPW increases. The average value of the T-type capacitor design also approaches the target value more closely. Calculations reveal that the offset of pattern has a negligible effect on J, and the coupling strength J remains stable in a range of d$L = \pm 0.5$ μm.

It is noteworthy that despite the C-type and T-type capacitors sharing the same structural shape, their sensitivity results are different from each other. These capacitor structures are equivalent to the mutual capacitance between the central electrode and surrounding electrodes, but they also encompass the self-capacitance between the central (or surrounding) electrode and the metal ground. The connection area of the T-type capacitor with the resonator is located in the center, and the average distance between the central electrode and the metal ground is large (~ 67 μm), while the surrounding electrodes are close to the metal ground (~ 12 μm). The self-capacitance fluctuation of the central electrode is minimal under fabrication variation, while the self-capacitance of the surrounding electrode exhibits significant fluctuation. The resonance frequency is mainly determined by the mutual capacitance, the

self-capacitances of the electrodes, and the coplanar waveguide part of the resonator. The T-type capacitor achieves optimal sensitivity of both mutual capacitance and ground capacitance simultaneously, so that the fluctuation of the resonant frequency is minimal, and the filter coupling parameters are highly stable. By suitably increasing the size of the CPW and employing a larger T-type capacitor structure, the coupling fluctuations caused by pattern edge deviations during fabrication can be mitigated, thereby leading to stable performance of Purcell filter devices.

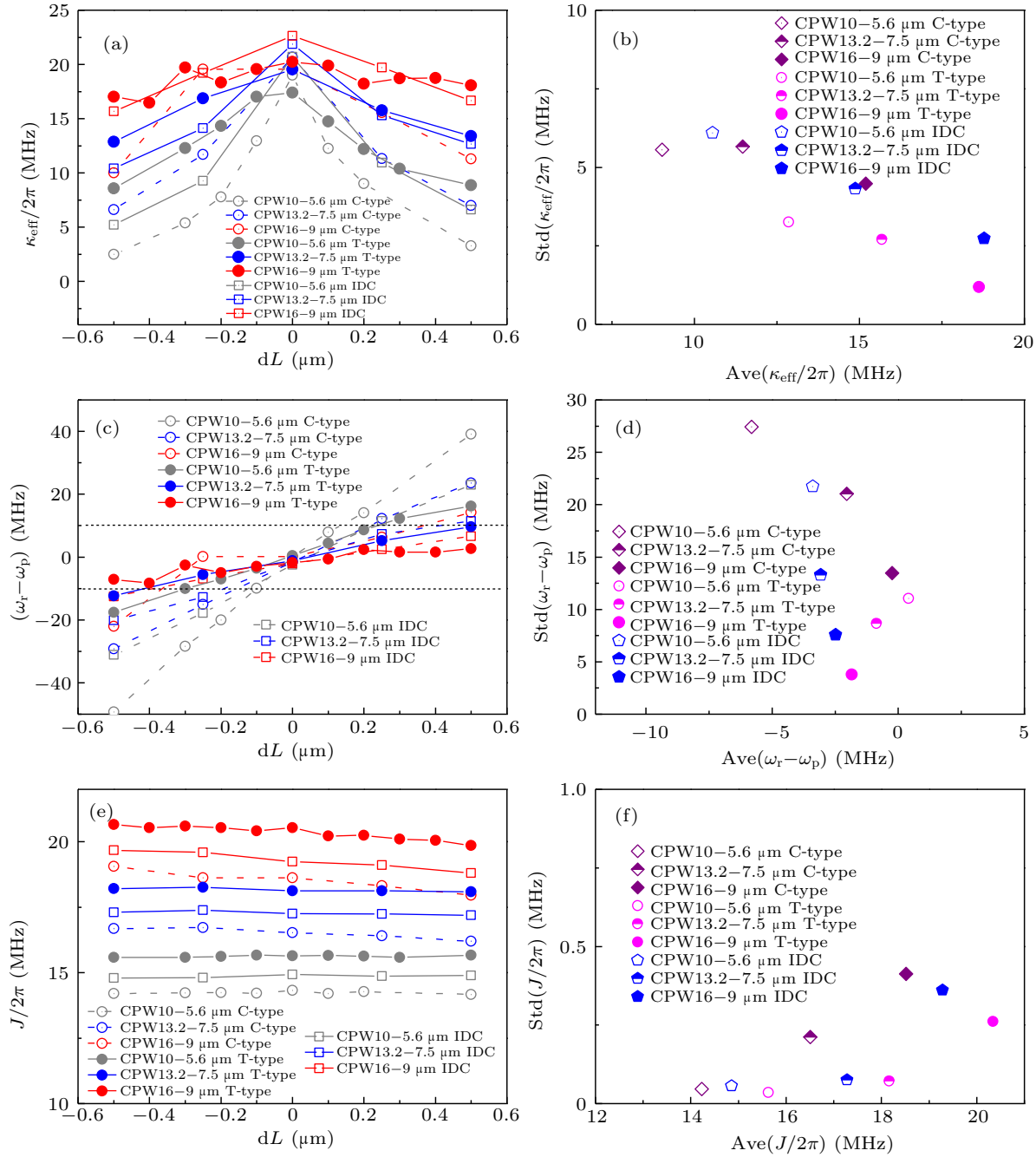


Fig. 4. Sensitivity analysis of filter coupling parameters and etching errors for multiple specifications of 50-Ω CPW structures with various 40-fF capacitor configurations, showing (a) correlations between CPW edge etching deviation (dL) and effective coupling strength $\kappa_{\rm eff}$, (b) average and standard deviations of $\kappa_{\rm eff}$ under different combinations, (c) correlations between dL and $\omega_{\rm r}-\omega_{\rm p}$, (d) average and standard deviations of $\omega_{\rm r}-\omega_{\rm p}$ under different combinations, (e) correlations between dL and coupling strength J, and (f) average and standard deviations of J under different combinations.

5. Conclusions

The stable and reliable performance of Purcell filter is crucial for qubit protection and rapid readout. This work systematically studies the main factors affecting the performance of individual Purcell filter during device preparation based on numerical analysis, by focusing on the structure of the coupling capacitor between the filter and the transmission line, as well as the CPW. The comparison with interdigital capacitors shows that using large-sized enclosing capacitors can reduce the sensitivity to structural edge fluctuations. By combining a

large CPW (w–s: 16 μm–9 μm) with a T-type enclosing capacitor structure ($L = 12$ μm) the effective coupling strength fluctuation of the device can be reduced to 10% with a maximum 0.5-μm edge deviation.

Acknowledgements

Project support by the Youth Innovation Promotion Association of the Chinese Academy of Sciences (CAS) (Grant No. 2019319), the Start-up Foundation of Suzhou Institute of Nano-Tech and Nano-Bionics, CAS, Suzhou, China (Grant No. Y9AAD110), the Innovative and Entrepreneurial Talents Project of Jiangsu Province, China (Grant No. JSSCBS20221743), and the Excellent Postdoctoral Talent Program of Jiangsu Province, China (Grant No. 2023ZB816).

References

[1] Wendin G 2017 *Rep. Prog. Phys.* **80** 106001
[2] McRae C R H, Wang H, Gao J, Vissers M R, Brecht T, Dunsworth A, Pappas D P and Mutus J 2020 *Rev. Sci. Instrum.* **91** 091101
[3] Kurter C, Murray C E, Gordon R T, Wymore B B, Sandberg M, Shelby R M, Eddins A, Adiga V P, Finck A D K, Rivera E, Stabile A A, Trimm B, Wacaser B, Balakrishnan K, Pyzyna A, Sleight J, Steffen M and Rodbell K 2022 *npj Quantum Inf.* **8** 31
[4] Wang C, Axline C, Gao Y Y, Brecht T, Chu Y, Frunzio L, Devoret M and Schoelkopf R J 2015 *Appl. Phys. Lett.* **107** 162601
[5] Place 2022 *Increasing Lifetimes of Superconducting Qubits* Ph.D. Dissertation (New Jersey: Princeton University)
[6] Sete E A, Martinis J M and Korotkov A N 2015 *Phys. Rev. A* **92** 012325
[7] Reed M D, Johnson B R, Houck A A, DiCarlo L, Chow J M, Schuster D I, Frunzio L and Schoelkopf R J 2010 *Appl. Phys. Lett.* **96** 203110
[8] Liu C H, Harrison D C, Patel S, Wilen C D, Rafferty O, Shearrow A, Ballard A, Iaia V, Ku J, Plourde B L T and McDermott R 2024 *Phys. Rev. Lett.* **132** 017001
[9] Pan X, Zhou Y, Yuan H, Nie L, Wei W, Zhang L, Li J, Liu S, Jiang Z H and Catelani G 2022 *Nat. Commun.* **13** 7196
[10] Sank D T 2014 *Fast, Accurate State Measurement in Superconducting Qubits* Ph.D. Dissertation, (California: University of California Santa Barbara)
[11] Neill C, Roushan P, Kechedzhi K, Boixo S, Isakov S V, Smelyanskiy V, Megrant A, Chiaro B, Dunsworth A and Arya K 2018 *Science* **360** 195
[12] Bronn N T, Liu Y, Hertzberg J B, Córcoles A D, Houck A A, Gambetta J M and Chow J M 2015 *Appl. Phys. Lett.* **107** 172601
[13] Jeffrey E, Sank D, Mutus J, White T, Kelly J, Barends R, Chen Y, Chen Z, Chiaro B and Dunsworth A 2014 *Phys. Rev. Lett.* **112** 190504
[14] Sunada Y, Kono S, Ilves J, Tamate S, Sugiyama T, Tabuchi Y and Nakamura Y 2022 *Phys. Rev. Appl.* **17** 044016
[15] Zhang X, Kim E, Mark D K, Choi S and Painter O 2023 *Science* **379** 278
[16] Yan H, Wu X, Lingenfelter A, Joshi Y J, Andersson G, Conner C R, Chou M H, Grebel J, Miller J M, Povey R G, Qiao H, Clerk A A and Cleland A N 2023 *Appl. Phys. Lett.* **123** 134001
[17] Iakoupov I and Koshino K 2023 *Phys. Rev. Res.* **5** 013148
[18] Salathé Y D 2018 *Toolbox for quantum computing and digital quantum simulation with superconducting qubits* Ph.D. Dissertation, (Zürich: ETH Zurich)
[19] Bronn N T, Magesan E, Masluk N A, Chow J M, Gambetta J M and Steffen M 2015 *IEEE Trans. Appl. Supercond.* **25** 1
[20] Heinsoo J, Andersen C K, Remm A, Krinner S, Walter T, Salathé Y, Gasparinetti S, Besse J C, Potočnik A and Wallraff A 2018 *Phys. Rev. Appl.* **10** 034040
[21] Vallés-Sanclemente S, van der Meer S L M, Finkel M, Muthusubramanian N, Beekman M, Ali H, Marques J F, Zachariadis C, Veen H M, Stavenga T, Haider N and DiCarlo L 2023 *Appl. Phys. Lett.* **123** 034004
[22] Cai X, Zhou B, Wu Y, Li S, Dong Y, Feng J and Xiong K 2023 *Supercond. Sci. Technol.* **36** 085001
[23] Reuer K, Landgraf J, Fösel T, O'Sullivan J, Beltrán L, Akin A, Norris G J, Remm A, Kerschbaum M, Besse J C, Marquardt F, Wallraff A and Eichler C 2023 *Nat. Commun.* **14** 7138
[24] Andersen C K, Remm A, Lazar S, Krinner S, Heinsoo J, Besse J C, Gabureac M, Wallraff A and Eichler C 2019 *npj Quantum Inf.* **5** 69
[25] Herrmann J, Llima S M, Remm A, Zapletal P, McMahon N A, Scarato C, Swiadek F, Andersen C K, Hellings C, Krinner S, Lacroix N, Lazar S, Kerschbaum M, Zanuz D C, Norris G J, Hartmann M J, Wallraff A and Eichler C 2022 *Nat. Commun.* **13** 4144